Electronic Supplementary Material

PdPt nanoparticles decorated thiol-functionalized MOF with high peroxidase-like activity for colorimetric sensing of D-glucose and chlorophenol isomers

Yuanqing Luo,‡ [a] [b] Shiwen Zhou,‡[a] Weiwei Chen,[a] Yaqin Liu,[a] Hongru Feng*[a] and Yuanjiang Pan*[a]

Author affiliations:

[a] Department of Chemistry, Zhejiang University, Hangzhou 310027, China

[b] College of Food Science and Engineering, Henan University of Technology, Zhengzhou 450001, China

* Corresponding authors

E-mail: panyuanjiang@zju.edu.cn, fenghongru@zju.edu.cn

‡ Equal contribution to this work.

Contents List

S1. Reagents and materials

2,5-dimercapto-1,4-benzenedicarboxylic acid (DMBD) was purchased from Yanshen Technology Co., Ltd. (JiLin, China). $Pd(OAc)_2$, Na_2HPO_4, NaH_2PO_4, K_2HPO_4, KH_2PO_4, 2-chlorophenol (2-CP), 4-chlorophenol (4-CP), 2,4-dichlorophenol (2,4-DCP), 2,5-dichlorophenol (2,5-DCP), and 3,5-dichlorophenol (3,5-DCP), $NaBH_4$, 2,2,6,6-tetramethylpiperidine (TEMP), 5,5-dimethyl-1-pyrroline-N-oxide (DMPO) were purchased from Aladdin Industrial Inc. (Shanghai, China). H_2O_2 (30 wt%), thiourea, and chloroplatinic acid hydrate ($H_2PtCl_6 \cdot 6H_2O$) were purchased from Sinopharm Chemical Reagent Co., Ltd. (Shanghai, China). $ZrCl_4$, *p*-benzoquinone, 3,4-dichlorophenol (3,4-DCP), 2,6-dichlorophenol (2,6-DCP), and 2,3-dichlorophenol (2,3-DCP) were purchased from Macklin Biochemical Co., Ltd. (Shanghai, China). 4-Aminoantipyrine (4-AAP), glucose oxidase (GOx), L-histidine, maltose, sucrose, lactose, fructose, and D-mannose were purchased from Yuanye Biotechnology Co., Ltd. (Shanghai, China). 3-chlorophenol (3-CP) was purchased from J&K chemicals (Beijing, China). D-glucose and L-glucose were purchased from Shanghai ZZBIO CO., Ltd. (Shanghai, China). Deionized water was prepared by a Milli-Q water purification system (Millipore, Billerica, MA, USA). All chemicals were analytical grade and above.

S2. Instrumentation and characterization

The morphologies and microstructures of the products were characterized by scanning electron microscopy (SEM), transmission electron microscopy (TEM) and high-resolution TEM (HRTEM). SEM images were recorded on Hitachi SU8010

(Japan). TEM images were taken with a Hitachi HT7700 (Japan) at an acceleration voltage of 100 kV. HRTEM images, selected area electron diffraction (SAED) pattern, scanning transmission electron microscopy (STEM), and dispersive X-ray analysis for elemental mapping (STEM-EDX) were collected on a Jeol JEM-2100F microscope (Japan). The XRD patterns determined by a powder X-ray diffraction (XRD) systems (Rigaku D/Max-2550pc) using Cu Kα radiation (λ = 0.1541 nm) at 40 kV and 250 mA in the 2θ ranging from 3° to 100° in steps of 0.02°. The X-ray photoelectron spectroscopy (XPS) measurements were carried out on an ESCALAB 250Xi spectrometer (Thermo Scientific, USA) equipped with a monochromatized Al Kα X-ray source. Zeta potential values were measured using the Zetasizer Nano-ZS (Malvern Instruments Ltd.) at 25 ℃. Fourier transform infrared (FTIR) spectra were recorded from KBr pellets in the range of 4000−400 cm^{-1} on a Nicolet iS10 spectrometer (Thermo Fisher Scientific, USA). The absorption spectra were recorded on a UV-1800 Ultraviolet-Visible (UV-Vis) spectrophotometer (Shimadzu, Tokyo, Japan) equipped with a 1 cm quartz cuvette (1.05 mL). The electron paramagnetic resonance (EPR) spectrum was measured using an A300 EPR spectrometer (Bruker, Germany). The commercial glucometer used was the Yuwell 580 glucometer. The pH measurements were carried out using a Metrohm pH-meter (model 780) with a combined pH glass electrode, calibrated against standard buffer solution with pH values of 4.01, 6.86, and 9.18 at 25℃.

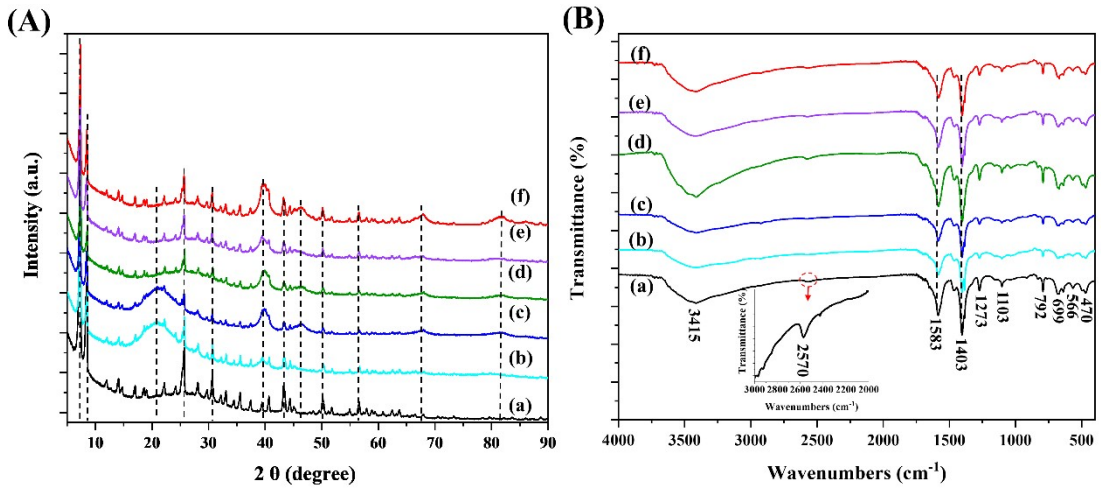

Fig. S1 XRD patterns (A) and FT-IR spectra (B) of UiO-66-$(SH)_2$ and UiO-66-$(SH)_2$@Pd_mPt_n (m : n = 1 : 0, 2 : 1, 1 : 1, 1: 2 and 0 : 1). (a) UiO-66-$(SH)_2$; (b) UiO-66-$(SH)_2$@Pd; (c)UiO-66-$(SH)_2$@Pt; (d)UiO-66-$(SH)_2$@Pd_1Pt_2; (e)UiO-66-$(SH)_2$@Pd_1Pt_1; (f)UiO-66-$(SH)_2$@Pd_2Pt_1.

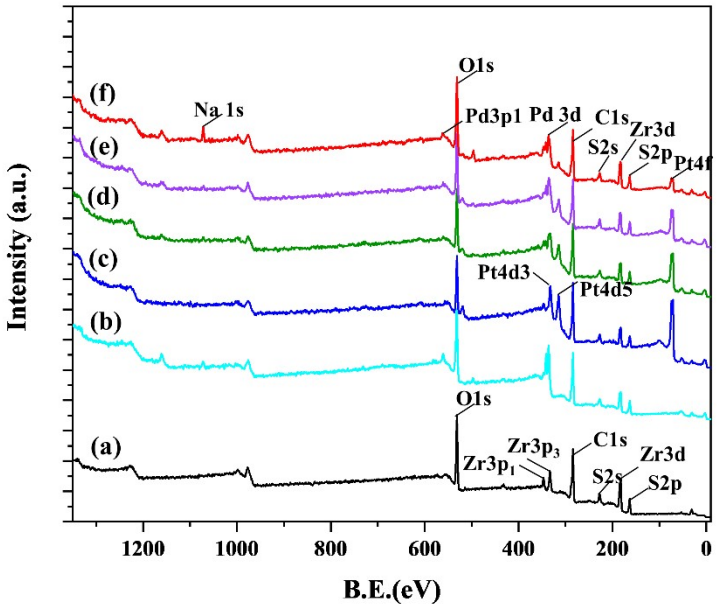

Fig. S2 XPS spectra of UiO-66-$(SH)_2$ and UiO-66-$(SH)_2$@Pd_mPt_n (m : n = 1 : 0, 2 : 1, 1 : 1, 1 : 2 and 0 : 1) (a) UiO-66-$(SH)_2$; (b) UiO-66-$(SH)_2$@Pd; (c)UiO-66-$(SH)_2$@Pt; (d)UiO-66-$(SH)_2$@Pd_1Pt_2; (e)UiO-66-$(SH)_2$@Pd_1Pt_1; (f)UiO-66-$(SH)_2$@Pd_2Pt_1.

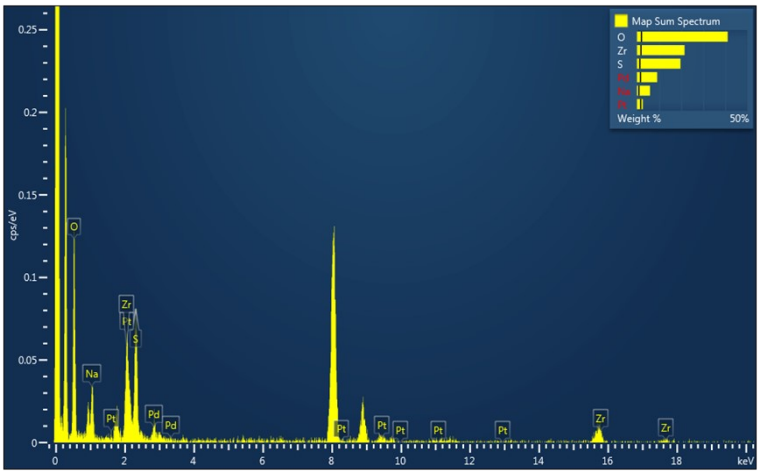

107

108 Fig. S3 Energy dispersive X-ray analysis of UiO-66-$(SH)_2$@Pd_2Pt_1.

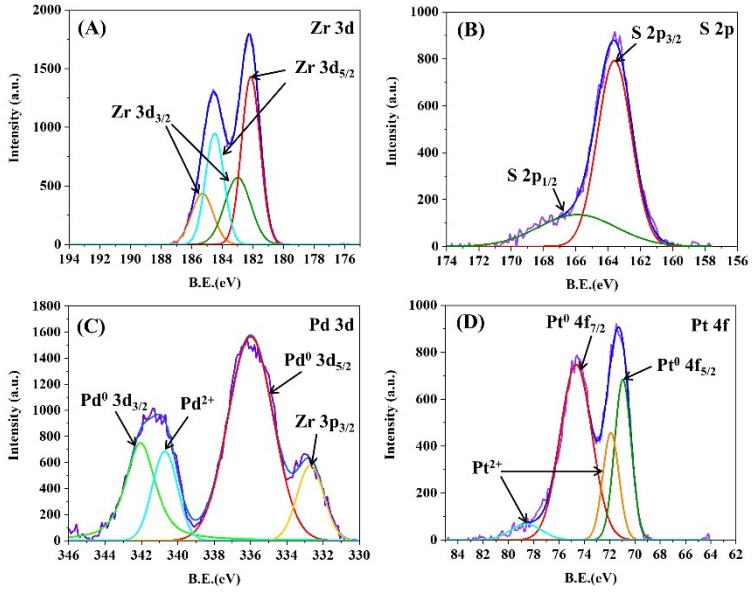

109

110 Fig. S4 High resolution XPS spectra of UiO-66-$(SH)_2$@Pd_2Pt_1: (A) Zr 3d; (B) S 2p; (C)

111 Pd 3d; (D) Pt 4f

112

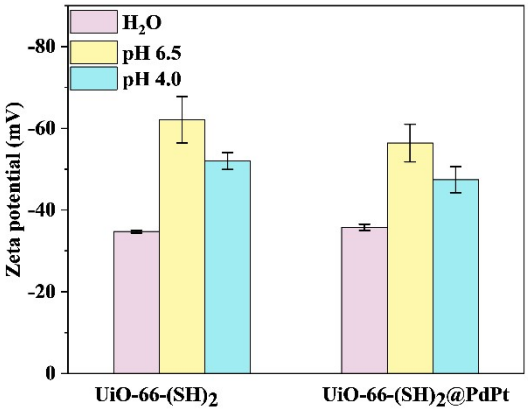

Fig. S5 Zeta potentials of UiO-66-$(SH)_2$ and UiO-66-$(SH)_2$@PdPtunder different conditions: H_2O, PBS (20 mM, pH = 6.5 and pH = 4.0).

S3. Experimental condition optimization for TMB oxidation

Similar to NEs, the enzymatic activity of NZs depends on the reaction time, pH, nanozyme concentration ([NZ]), and temperature. As shown in **Fig. S6 A**, the absorbance gradually increased with increasing reaction time and then leveled off after 15 min. The increasing relationship between absorbance and time was close to linear correlation within 5 min. The POD-like activity was also influenced by the reaction temperature (**Fig. S6 B**). The catalytic activity of the NZ gradually increased in the range of 25–60 °C, exhibiting the highest catalytic activity (100%) up to 60 °C. It suggested that the NZ has good thermal stability. In the range of 60–90 °C, the catalytic activity of the NZ sharply decreased to 13.0%. The catalytic activity was maintained at 61.9% at room temperature (25°C) relative to the optimum activity. To facilitate the operation, subsequent experiments were carried out at room temperature. Besides, the catalytic activity of the NZ was also affected by the NZ concentration ([NZ]). As shown in **Fig. S6 C**, the catalytic activity increased gradually in the [NZ] range of 1–50 $\mu g \cdot mL^{-1}$. However, as the [NZ] increased, the native color of the NZ caused interference with

the oxidative color development of TMB. Since the catalytic activity of UiO-66-$(SH)_2$@PdPt remained at 80.0% at a concentration of 25 $\mu g \cdot mL^{-1}$, and the interference of the background color on the color development reaction was almost negligible at this concentration. Therefore, the [NZ] was fixed at 25 $\mu g \cdot mL^{-1}$ in the subsequent reaction. The POD-like activity of the NZ was studied in the pH range from 2.5 to 8.0 (**Fig.S6 D**), and the results showed that the NZ displayed the best catalytic activity at pH = 4.0. The catalytic activity remained at 70.0 % at near-neutral condition of pH = 6.5, while it decreased to 22.1 % at the weakly basic conditions of pH = 8.0. Further, the oxidase-like activity of UiO-66-$(SH)_2$@PdPt was also studied in the same pH range. The results showed that the oxidase-like activity exhibited optimal activity only in the moderately acidic pH range (2.5–5.0), while at pH ≥ 6.5, the oxidative activity decreased to below 5% which was almost negligible(**Fig.S6 E**). Therefore, to eliminate the interference of intrinsic oxidase-like activity, subsequent studies of POD-like activity were performed in a near-neutral (pH = 6.5) PBS buffered (20 mM) system.

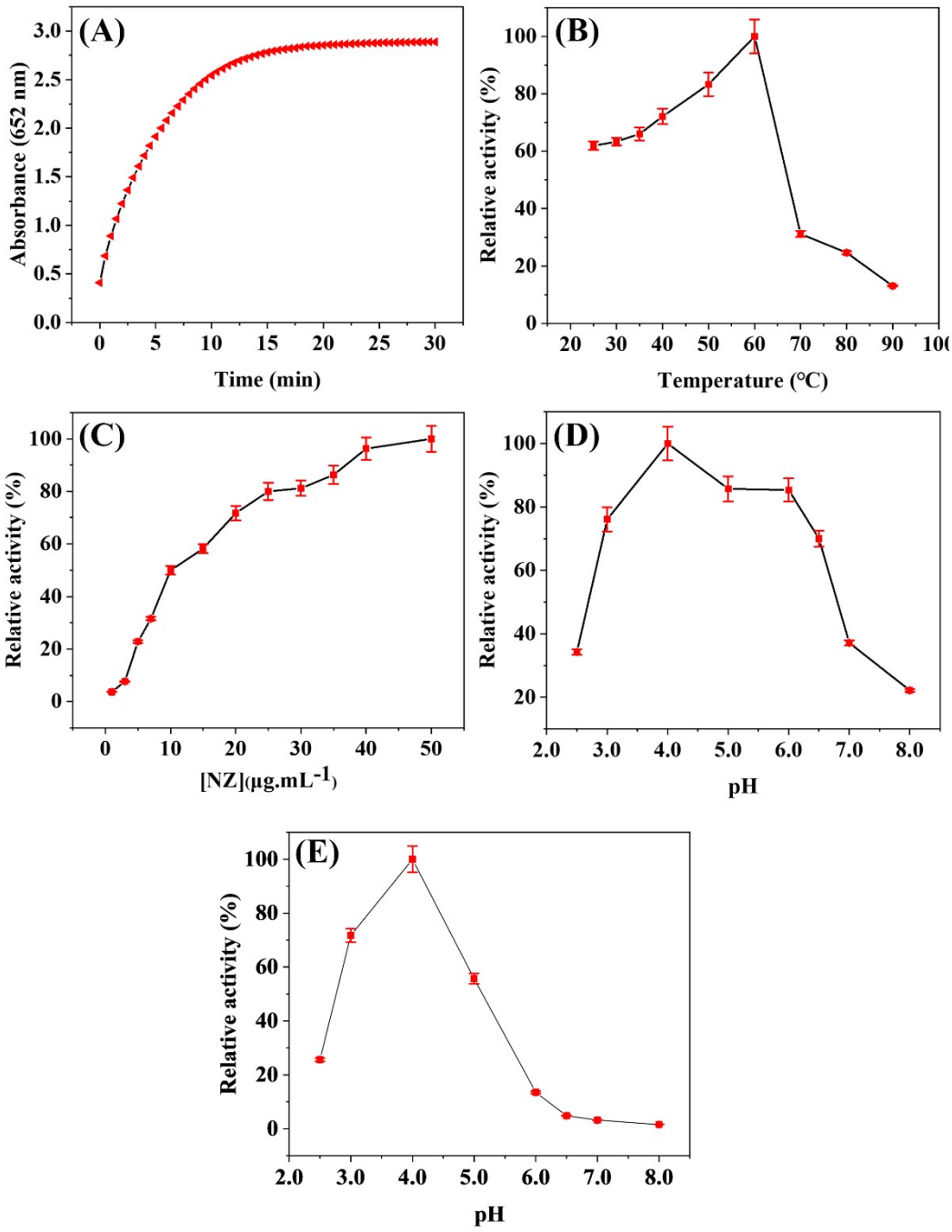

Fig. S6 Dependence of UiO-66-$(SH)_2$@PdPt + H_2O_2 + TMB oxidation system on reaction time (A); temperature (B); nanozyme concentration([NZ]) (C) and pH (D), and dependence of UiO-66-$(SH)_2$@PdPt + TMB oxidation system on reaction pH (E). (error bar was obtained from three parallel experimental values).

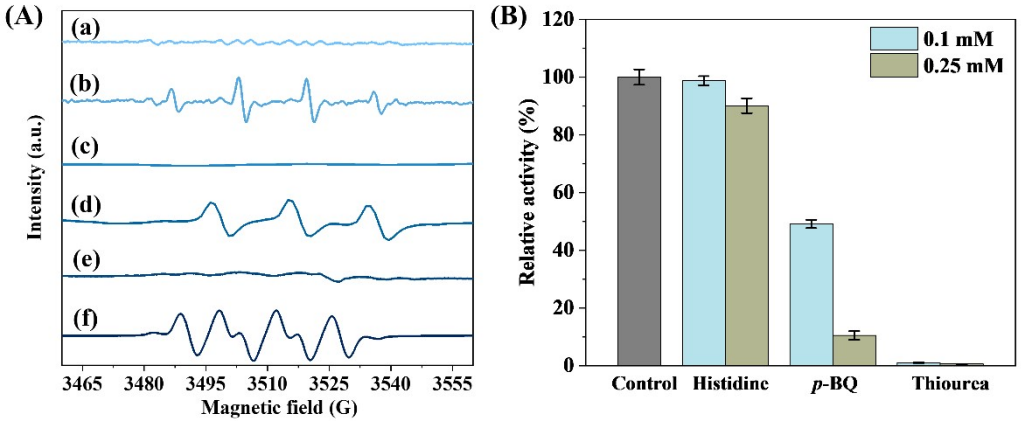

Fig. S7 (A) EPR spectra of UiO-66-$(SH)_2$@Pd_2Pt_1 for •OH, $^1O_2$, $O_2^{\bullet-}$ and their blank controls: (a) DMPO + H_2O_2 + PBS; (b) DMPO + H_2O_2 + NZ + PBS; (c) TEMP+ H_2O_2 + PBS; (d) TEMP+ H_2O_2+ NZ + PBS; (e) DMPO+ H_2O_2 + methanol; (f) DMPO + H_2O_2 + NZ + methanol. Reaction conditions: NZ (75 μg/mL), H_2O_2 (1 mM), PBS (pH = 6.5, 20 mM), room temperature, 5-10 min. (B) Effects of ROS radical scavengers (Histidine, *p*-BQ and Thiourea) on TMB-H_2O_2-UiO-66-$(SH)_2$@PdPt reaction system at pH = 6.5 (error bars were obtained based on three parallel experiments). Reaction conditions: 865 μL PBS (pH = 6.5, 20 mM), 20 μL radical scavenger (0, 5, or 12.5 mM), 50 μL H_2O_2 (20 mM), 40 μL TMB (15 mM), 25 μL UiO-66-$(SH)_2$@PdPt (1 mg/mL), 25℃, 5 min.

S4. Experimental condition optimization for the oxidative coupling reaction of 2-CP and 4-AAP

Interestingly, unlike TMB as a substrate, the optimal reaction pH for UiO-66-$(SH)_2$@PdPt catalyzed oxidation reaction with 2-CP and 4-AAP as substrates was 6.5 while that of the former was 4.0 (Fig. S8 A). This difference may be the consequence of two factors: on the one hand, differences in substrates may lead to changes in reaction conditions. The physicochemical properties of 2-CP and TMB differ significantly, e.g.,

the p*K*a value of 2-CP ranges from 8.3 to 8.6, whereas the p*K*a value of TMB is 4.49[1, 2]; On the other hand, the color development reaction was also influenced by the coupling step of the quinone product with 4-AAP. Near-neutral conditions favor the stable presence of the quinoneimine structure. The optimal concentration of 4-AAP was determined as 1 mg·mL^{-1} (**Fig. S8 B**). The reaction activity increased as the H_2O_2 concentration increased and reached saturation after 20 mM, thus this concentration was determined to be the optimal concentration of H_2O_2 (**Fig. S8 C**). Considering the background interference, convenience and time cost of the assay, the reaction was carried out at room temperature with a reaction time of less than 30 min and the concentration of NZ was kept at 25 μg· mL^{-1} (**Figs. S8 D and E**).

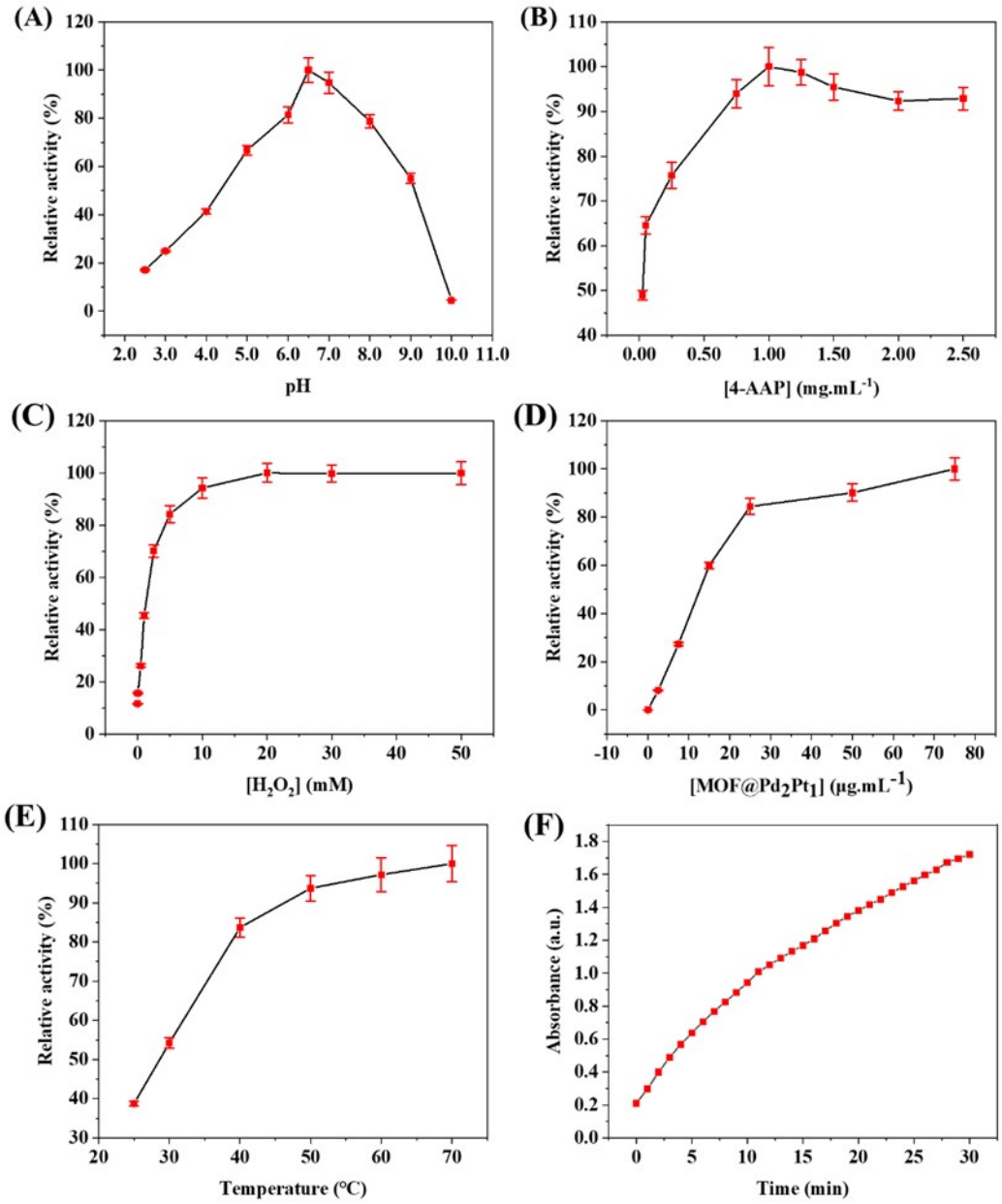

186

187 Fig. S8 Dependence of UiO-66-$(SH)_2$@PdPt + H_2O_2 + 4-AAP + 2-CP system on pH

188 (A); 4-AAP concentration (B); H_2O_2 concentration (C); nanozyme concentration (D);

189 temperature (E) and reaction time (F).

190

191

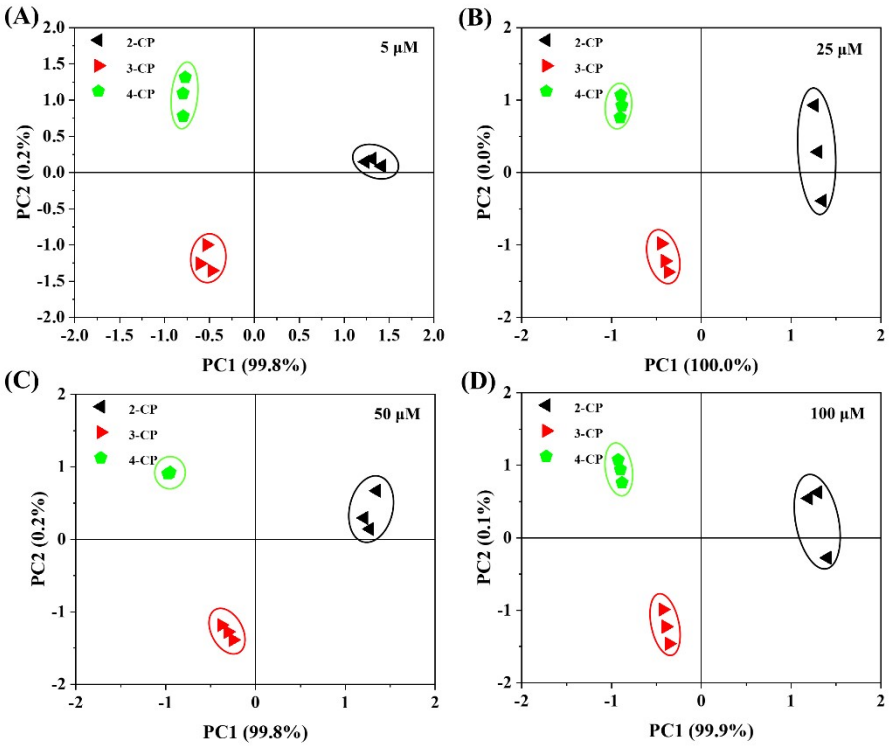

192

193 Fig. S9 PCA score maps of response modes for three CP isomers of 5 μM (A), 25 μM

194 (B), 50 μM (C) and 100 μM (D).

195

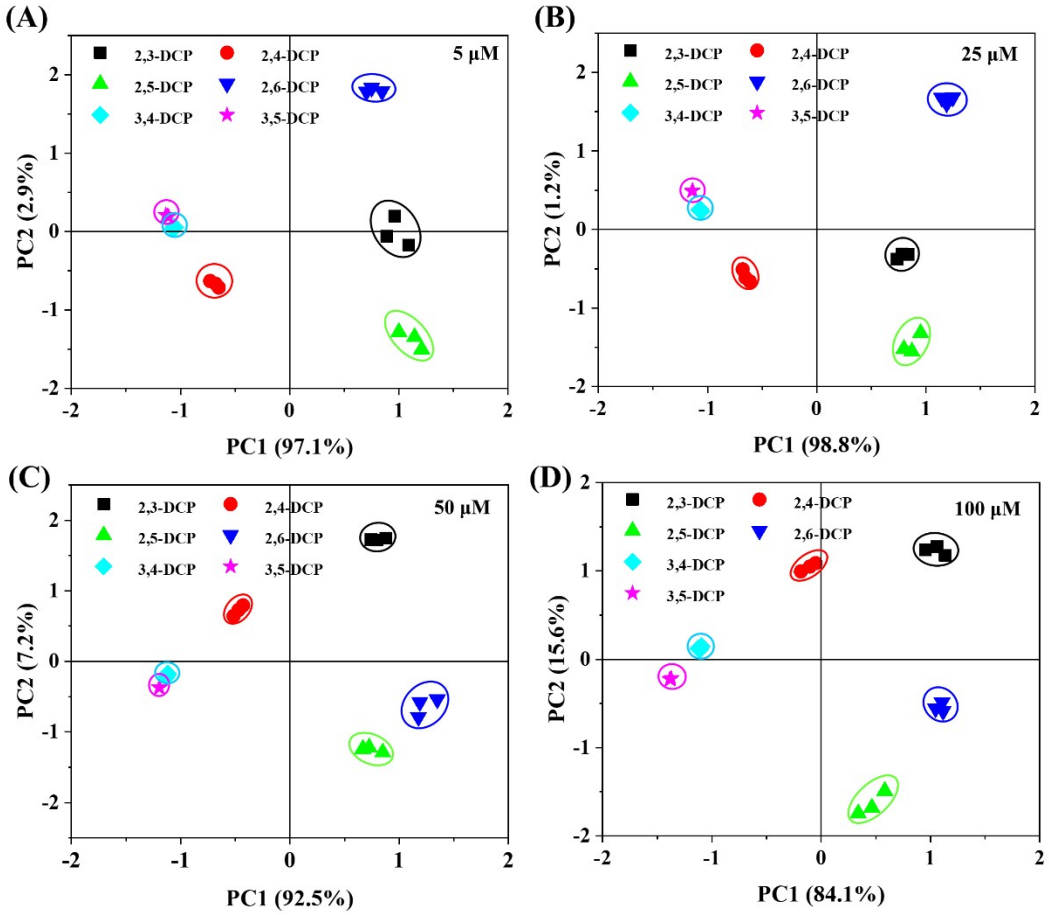

196

197 Fig. S10 PCA score maps of response modes for six DCP isomers of 5 μM (A), 25 μM

198 (B), 50 μM (C) and 100 μM (D).

199

200

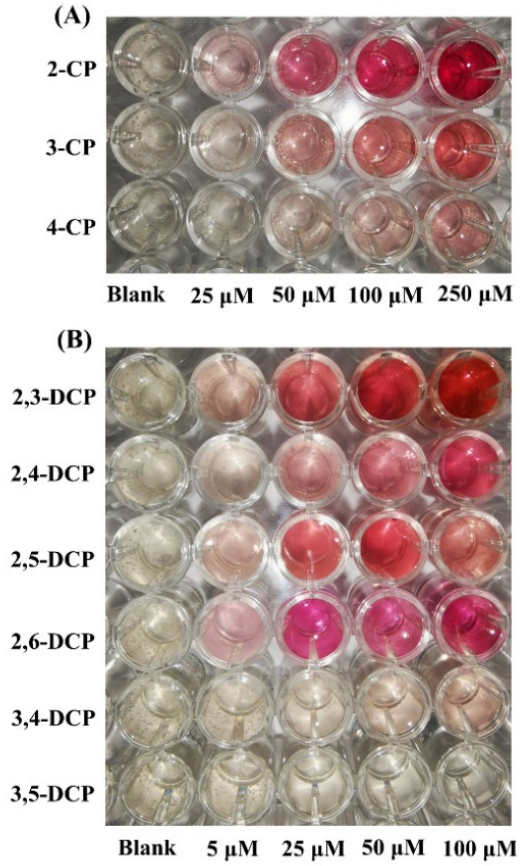

Fig. S11 Color response of UiO-66-$(SH)_2$@PdPt + H_2O_2 + 4-AAP system in the presence of CPs (A) and DCPs (B) at different concentrations.

Table S1 Kinetic parameters of catalytic reaction between different nanozymes and HRP.

Catalyst	K_m (Mm)		V_{max} ($\times 10^{-8}$ M·s^{-1})		Ref.
	TMB	H_2O_2	TMB	H_2O_2	
HRP	0.434	3.70	10.0	8.71	[3]
Fe_3O_4 MNPs	0.098	154	3.44	9.78	[3]
2D Pd@Pt	0.0865	2.231	6.228	5	[4]
Dap-$Pd_{0.25}$ NPs	0.4	2.636	4.61	1.837	[5]
GeO_2	0.420	1.75	23.397	23.400	[6]
Ru@G	0.027	5.8	163	13.7	[7]
Cu/Au/Pt TNPs	0.15	2.34	7.33	136.5	[8]
Graphene-Au NPs	0.38	26.4	18.30	15.41	[9]
Pt_{200}-JP	0.719	9.344	51.33	12.49	[10]
NAC-Pt_8	0.132	35.00	48.15	31.23	[11]
Pt NP	0.127	1.14	2	3.1	[12]
Pd-Ir cubes	0.13	0.034	6.5	5.1	[13]
Fe_3O_4@SiO_2-NH_2-Au@$Pd_{0.30}$NPs	0.090	3.50	11.20	6.76	[14]
MSN-AuNPs	0.0411	15.81	12.66	17.30	[15]
UiO-66-$(SH)_2$@PdPt	0.068	1.25	15.51	20.28	This work

222 Table S2 The performance of the nanozyme for glucose colorimetric detection.

Nanozyme	Linear range (μM)	LOD (μM）	pH	Ref.
WS_2	5–300	2.9	6.9	[16]
CuS	25–600	4.9	7	[17]
FeCPNPs	2–20	1	7	[18]
Hep-Pt	100–2000	33	6.0	[19]
$MoSe_2$ nanosheets	40–400	28	7.0	[20]
$SO_4^{2-}/CoFe_2O_4$	0–300	6.4	7.0	[21]
$Cu_{0.89}Zn_{0.11}O$	25–500	1.5	4.65	[22]
WSe_2 nanosheets	10-60	10	3.5	[23]
CeO_2/Y	0–340	35.4	3.6	[24]
MoS_2 NPs	15–135	7	3.5	[25]
H_2TCPP-Fe_3O_4	5–25	2.21	3.8	[26]
Pt-CMP	5–100	0.12	4.0	[27]
Por-Ceria	40–150	19	3.8	[28]
GK-Pd NPs	10–1000	6	4.0	[29]
Fe_3O_4 MNPs	50–1000	30	4.0	[30]
UiO-66-$(SH)_2$@PdPt	5–700	2.7	6.5	This work

223

224

225

226

227

228 Table S3 Determination of D-glucose concentration in human serum.

Human serum	Proposed method	Glucometer	Relative

sample	(mM，*n*=3)	（mM）	error（%)
Sample 1	4.04 ± 0.08	4.1	-1.46
Sample 2	5.99 ± 0.33	6.2	-3.39
Sample 3	7.62 ± 0.20	7.8	-2.31
Sample 4	11.71 ± 0.23	11.9	-1.60
Sample 5	15.47 ± 0.10	15.6	-0.83

229

230 Table S4 The performance of different methods for the detection of 2-CP or 2,4- DCP.

Material	Method	Analyte	Linear range（μM）	LOD（μM）	Ref.
Fe_3O_4 NPs	Chromatographic	2-CP	0.5 – 50	0.15	[31]
Fe_3O_4@MnO_x	Colorimetric	2-CP	0.1 – 10，10 – 1600	0.85	[32]
CNT-PPy-HRP	Electrochemical	2-CP	1.6 – 8.0	0.26	[33]
Poly(GMA-co-MTM)/PPy/CNT	Electrochemical	2-CP	1.6 – 68.8	0.249	[34]
g-C_3N_4/CDs/GCE	Electrochemical	2-CP	0.5 – 10	1.50	[35]
Cu–BTC/GO	Electrochemical	2,4-DCP	1.5 – 24	0.083	[36]
[Cu(bpy)(H_2O)$_2$(BF_4)$_2$(bpy)]	Electrochemical	2,4-DCP	4 – 100	1.1	[37]
Fe_1@CN-20	Colorimetric	2,4-DCP	30 – 184	1.3	[38]
UiO-66-$(SH)_2$@PdPt	Colorimetric	2-CP	0.5 – 200	0.24	This work
UiO-66-$(SH)_2$@PdPt	Colorimetric	2,4-DCP	0.5 – 200	0.41	This work

231 Table S5 Determination of 2-CP and 2,4- DCP in spiked samples.

Spiked	Concentration (μM)	Found (μM)	RSD(%, *n*=3)	Recovery(%)

2-CP	25	25.76 ± 0.67	2.6	103.0
	50	51.67 ± 2.17	4.2	103.3
	100	93.32 ± 2.89	3.1	93.3
2,4-DCP	25	24.22 ± 0.56	2.3	96.9
	50	44.45 ± 0.42	0.96	88.9
	100	112.21 ± 5.66	5.1	112.2

232

233 **Reference**

234 1. K. C. Yang, Y. X. Zhao, M. Ji, Z. L. Li, S. Y. Zhai, X. Zhou, Q. Wang, C. Wang and
235 B. Liang, *Water Res.*, 2021, **193**.
236 2. Z. N. Garba, W. M. Zhou, I. Lawan, W. Xiao, M. X. Zhang, L. W. Wang, L. H. Chen
237 and Z. H. Yuan, *J. Environ. Manage.*, 2019, **241**, 59-75.
238 3. L. Z. Gao, J. Zhuang, L. Nie, J. B. Zhang, Y. Zhang, N. Gu, T. H. Wang, J. Feng, D.
239 L. Yang, S. Perrett and X. Yan, *Nat. Nanotechnol.*, 2007, **2**, 577-583.
240 4. J. P. Wei, X. L. Chen, S. G. Shi, S. G. Mo and N. F. Zheng, *Nanoscale*, 2015, **7**,
241 19018-19026.
242 5. Y. Liang, H. C. Li, L. Y. Fan, R. Y. Li, Y. S. Cui, X. B. Ji, H. Y. Xiao, J. Hu and L.
243 G. Wang, *Colloid. Surface. A*, 2022, **633**.
244 6. X. Liang and L. Han, *Adv. Funct. Mater.*, 2020, **30**.
245 7. P. Keoingthong, Q. Hao, S. K. Li, L. Zhang, J. Q. Xu, S. Wang, L. Chen, W. H. Tan
246 and Z. Chen, *Chem. Commun.*, 2021, **57**, 7669-7672.
247 8. P. Wu, P. Ding, X. S. Ye, L. Li, X. X. He and K. M. Wang, *RSC Adv.*, 2019, **9**,
248 14982-14989.
249 9. X. M. Chen, X. T. Tian, B. Y. Su, Z. Y. Huang, X. Chen and M. Oyama, *Dalton T.*,
250 2014, **43**, 7449-7454.
251 10. X. L. Guo, Y. X. Suo, X. Zhang, Y. S. Cui, S. F. Chen, H. T. Sun, D. W. Gao, Z.
252 W. Liu and L. G. Wang, *Analyst*, 2019, **144**, 5179-5185.
253 11. X. X. Li, Q. W. Huang, W. Li, J. L. Zhang and Y. Fu, *J Anal Test*, 2019, **3**, 277-
254 285.
255 12. A. J. Kora and L. Rastogi, *Sens. Actuat B-Chem.*, 2018, **254**, 690-700.

13. X. H. Xia, J. T. Zhang, N. Lu, M. J. Kim, K. Ghale, Y. Xu, E. McKenzie, J. B. Liu and H. H. Yet, *Acs Nano*, 2015, **9**, 9994-10004.
14. O. Adeniyi, S. Sicwetsha and P. Mashazi, *Acs Appl. Mater. Inter.*, 2020, **12**, 1973-1987.
15. Y. Tao, E. G. Ju, J. S. Ren and X. G. Qu, *Adv. Mater.*, 2015, **27**, 1097-1104.
16. T. R. Lin, L. S. Zhong, Z. P. Song, L. Q. Guo, H. Y. Wu, Q. Q. Guo, Y. Chen, F. F. Fu and G. N. Chen, *Biosens. Bioelectron.*, 2014, **62**, 302-307.
17. X. H. Niu, X. C. Xu, X. Li, J. M. Pan, F. X. Qiu, H. L. Zhao and M. B. Lan, *Chem. Commun.*, 2018, **54**, 13443-13446.
18. J. Q. Tian, S. Liu, Y. L. Luo and X. P. Sun, *Catal. Sci. Technol.*, 2012, **2**, 432-436.
19. H. Z. Gu, Q. W. Huang, J. L. Zhang, W. Li and Y. Fu, *Colloid. Surface. A*, 2020, **606**.
20. G. Y. Jiang, T. R. Lin, Y. X. Qin, X. H. Zhang, L. Hou, Y. Sun, J. J. Huang, S. D. Liu and S. L. Zhao, *Chem. Commun.*, 2020, **56**, 10847-10850.
21. X. L. Yin, P. Liu, X. C. Xu, J. M. Pan, X. Li and X. H. Niu, *Sens. Actuat B-Chem.*, 2021, **328**.
22. A. P. Nagvenkar and A. Gedanken, *Acs Appl. Mater. Inter.*, 2016, **8**, 22301-22308.
23. T. M. Chen, X. J. Wu, J. X. Wang and G. W. Yang, *Nanoscale*, 2017, **9**, 11806-11813.
24. X. W. Cheng, L. Huang, X. Y. Yang, A. A. Elzatahry, A. Alghamdi and Y. H. Deng, *J. Colloid. Interf. Sci.*, 2019, **535**, 425-435.
25. Y. H. Zhao, Y. Huang, J. L. Wu, X. L. Zhan, Y. Y. Xie, D. Y. Tang, H. Y. Cao and W. Yun, *RSC Adv.*, 2018, **8**, 7252-7259.
26. Q. Y. Liu, H. Li, Q. R. Zhao, R. R. Zhu, Y. T. Yang, Q. Y. Jia, B. Bian and L. H. Zhuo, *Mat. Sci. Eng. C-Mater.*, 2014, **41**, 142-151.
27. G. Q. Wang, L. S. Feng, W. Li, J. L. Zhang and Y. Fu, *Microchim. Acta*, 2019, **186**.
28. Q. Y. Liu, Y. T. Yang, X. T. Lv, Y. A. Ding, Y. Z. Zhang, J. J. Jing and C. X. Xu, *Sens. Actuat B-Chem.*, 2017, **240**, 726-734.
29. L. Rastogi, D. Karunasagar, R. B. Sashidhar and A. Giri, *Sens. Actuat B-Chem.*, 2017, **240**, 1182-1188.

30. H. Wei and E. Wang, *Analytical Chemistry*, 2008, **80**, 2250-2254.
31. J. D. Li, X. L. Zhao, Y. L. Shi, Y. Q. Cai, S. F. Mou and G. B. Jiang, *J. Chromatogr. A*, 2008, **1180**, 24-31.
32. X. C. Xu, S. W. Wu, D. Z. Guo and X. H. Niu, *Anal. Chim. Acta*, 2020, **1107**, 203-212.
33. S. Korkut, B. Keskinler and E. Erhan, *Talanta*, 2008, **76**, 1147-1152.
34. S. K. Ozoner, F. Yilmaz, A. Celik, B. Keskinler and E. Erhan, *Curr. Appl. Phys.*, 2011, **11**, 402-408.
35. T. H. G. Moundzounga, M. G. Peleyeju, S. O. Sanni, M. J. Klink, E. Oseghe, E. Viljoen and A. E. Ofomaja, *Int. J. Electrochem. Sci.*, 2021, **16**, 210560.
36. M. B. Nguyen, V. T. Hong Nhung, V. T. Thu, D. T. Ngoc Nga, T. N. Pham Truong, H. T. Giang, P. T. Hai Yen, P. H. Phong, T. A. Vu and V. T. Thu Ha, *RSC Adv.*, 2020, **10**, 42212-42220.
37. M. Cui, J. Li, D. Lu and Z. Shao, *Int. J. Electrochem. Sci.*, 2018, **13**, 3420-3428.
38. Y. M. Lin, F. Wang, J. Yu, X. Zhang and G. P. Lu, *J. Hazard. Mater.*, 2022, **425**.